# Constraint-Independent CTOA Determination for Stable Crack Growth in High Strength Ductile Steels

#### Xian-Kui Zhu

Materials Technology and Energy Science, Savannah River National Laboratory, Aiken, SC 29808, USA

**ABSTRACT:** Crack tip opening angle (CTOA) is one of fracture toughness parameters used for decades in describing large stable crack growth for thin-walled aerospace structures under the low-constraint conditions. Recently, the pipeline industry had a growing interest to use the CTOA parameter to serve as the minimum required fracture toughness to arrest a dynamic crack propagating in a modern gas transmission pipeline made of high strength ductile steel. The CTOA test standard ASTM E3039 was thus developed for measuring a constant critical CTOA to meet this industry need. ASTM E3039 recommends a drop weight tearing test (DWTT) specimen with a shallow crack for the standard CTOA testing, but its CTOA may depend on the low constraint condition at the crack tip for the DWTT specimen. Verifying the constraint independence of the DWTT measured CTOA thus becomes indispensable for applying the CTOA toughness to the running fracture control in the pipeline design. For this purpose, the present paper evaluates the critical CTOA values for a set of fracture toughness tests on single edge notched bend (SENB) specimens with shallow and deep cracks based on four CTOA estimation models. Among them, the Ln(P)-LLD linear fit model is similar to that recommended by ASTM E3039 for the CTOA calculation. Fracture test data for X80 pipeline steel and for HY80 structural steel are considered in the CTOA evaluation. The results show that the four CTOA models can determine a constraint independent CTOA value over stable crack growth for the SENB specimens. As a result, a single, reliable, constant CTOA value is determined regardless of the specimen geometry or the crack-tip constraint conditions. Therefore, the CTOA measured by ASTM E3039 is constraint-independent and transferable to use for an actual crack propagating in a gas transmission pipeline.

Keywords: fracture toughness; CTOA; constraint effect; DWTT; SENB; crack propagation

#### 1. Introduction

Fracture mechanics methods play an indispensable role in engineering structural design and asset integrity management for large-scale nation's infrastructure, including pressure vessels and transmission pipelines. These pressure components are commonly made of either stainless steels or carbon steels, and both steels have good ductility against crack initiation or growth. For these ductile steels, the elastic-plastic fracture mechanics methods are often utilized in an engineering critical analysis (ECA), with fracture toughness of the material characterizing by one of fracture parameters: J-integral [1], crack tip opening displacement (CTOD) [2], and crack tip opening angle (CTOA) [3]. Originally, the J-integral was proposed to describe the intensity of singularity of the crack-tip field for a ductile material, CTOD was proposed to describe the capability of ductile crack opening, and CTOA was introduced to simulate stable crack growth in a ductile material for finite element analysis (FEA). Since the 1980s, these fracture parameters have also been used to describe fracture toughness of ductile materials against crack initiation or growth. Over the past decades, many fracture toughness measurement methods have been developed and standardized worldwide by different organization, such as American Society for Testing and Materials (ASTM) for

metallic materials, as comprehensively reviewed by Zhu and Joyce [4]. Two commonly used standard fracture specimens for toughness testing are compact tension (CT) and single edge notched bend (SENB) specimens. ASTM E399 [5] was the first developed standard for testing the plane strain fracture toughness Kic, and ASTM E1820 [6] was then developed for testing plane strain initiation toughness or resistance curves in terms of the J-integral or CTOD, where CTOD is converted from the J-integral. For non-standard fracture specimens, Zhu [7] presented a technical review on the fracture toughness test methods in the low constraint conditions.

The J-integral and CTOD parameters are typically utilized to describe crack initiation and small stable crack growth [4], where the CTOD parameter is often employed to describe fracture toughness for pipeline girth welds [8-9]. In contrast, the CTOA parameter is particularly employed to describe the fracture resistance against large stable crack growth for ductile steels [4]. Actually, the CTOA parameter has been used for decades as a reliable fracture toughness parameter to characterize large stable crack growth for thin-walled aerospace structures in the low-constraint conditions [10]. ASTM developed the first CTOA test standard E2472 [11] in 2006 for thin-walled CT and middle-crack tension (MT) specimens, where CTOA is directly measured on the specimen surfaces using a surface measurement technology, such as digital image correction [12] or optical measurement methods [13]. In recent years, the pipeline industry started to use a constant CTOA as the arrest fracture toughness parameter to control and prevent a dynamic crack propagation in modern gas transmission pipelines [13 – 21]. For a gas pipeline, the wall thickness typically ranges from 6.5 mm to 20 mm that is considerably larger than the wall thickness (e.g., 5 mm or less) for aerospace structures. As a result, a surface CTOA measured using ASTM E2472 [11] may be not applicable to gas pipelines due to thicker walls. Experiments also showed that the CTOA measured at the midplane of a thicker fracture specimen can be significantly smaller than the surface CTOA measured for the thicker fracture specimen [21-22]. Thus, a constant midplane CTOA would be more appropriate to use for gas transmission pipelines. For this purpose, Martinelli and Venzi [23] developed an approximate model for estimating CTOA from the post-peak absorbed energy that was calculated from load-displacement data measured from a single SENB specimen test. After modification, Xu et al. [24] proposed a simplified single specimen method that can infer a more accurate CTOA value using the load-displacement data from a thicker drop weight tear test (DWTT) specimen test. On this basis, ASTM developed a second CTOA test standard E3039 [25] in 2016 for measuring a constant CTOA for ferritic steels at the midplane of the DWTT specimen. This DWTT specimen has an initial shallow crack, corresponding to the low-constraint condition at the crack tip. Without further study, it is unknown if the ASTM E3039 measured CTOA is constraintdependent or constraint-independent.

Constraint dependent fracture toughness is often known as constrain effect on fracture toughness. The transferability issue of fracture toughness refers if the laboratory measured fracture toughness is directly applicable to an actual crack without a constraint correction. The transferability of fracture toughness holds true when the laboratory measured fracture toughness is constraint independent. Otherwise, a constraint correction on the measured fracture toughness must be considered to ensure the constraint condition at an actual crack tip matching that for the laboratory fracture specimen. In order to prove the transferability of CTOA measured by the ASTM E3039 standard, many researchers [26-32] studied the constraint dependence of CTOA measured from DWTT specimens or full-scale tests on different ductile steels using experimental and numerical methods.

Parmar et al. [26] performed two FEA simulations on shallowly cracked DWTT specimens in three-point bending and in remote tension, respectively. The FEA results showed that the DWTT specimen in bending has a much higher constraint level at the crack tip than the DWTT specimen in tension. However, the critical CTOA values from these two loading conditions are comparable to the ASTM E3039 DWTT measured CTOA of 12.4° for X70 pipeline steel. It is concluded that "the crack-tip constraint condition has

a negligible effect on the critical CTOA for the X70 pipeline steel". In other word, the DWTT measured CTOA at the midplane is constraint independent. Recently, Zhen et al. [27] carried out a full-scale test (FST) on STPG370 carbon steel and performed the corresponding FEA simulation of CTOA for the burst tested pipe. The results demonstrated that the critical CTOA obtained from the FEA simulation was verified by the FST experimental data.

Recently, Jiao et al. [28] analyzed the dependency of the critical CTOA on the fracture speed obtained from different DWTT specimens for X80, with the CTOA decreasing as the fracture speed increases in the transition region of DWTT specimens. Note that the CTOA values were measured on the DWTT specimens using the high speed cameras. Further study by Xu et al. [29] showed that (1) "the critical CTOA is insensitive to the fracture speed for the pipeline steel in the steady-state region of DWTT specimens that is relevant to the ductile fracture propagation in the gas pipeline", and (2) "the ASTM E3039 determined CTOA is lose to the measured CTOA at the midplane of DWTT specimen". In addition, Paermentier et al. [30] designed a dynamic tensile tear test (DT3) specimen that resembles the actual loading conditions of inservice pipeline and conducted dynamic crack propagation tests to measure the critical CTOA for X70 pipeline steel. Their test results showed that the measured CTOA during the steady-state crack propagation in the DT3 specimens is a constant about 8° for the X70 pipeline steel.

To further study the CTOA transferability, Shibanuma et al. [31] carried out a series of impact tests on DWTT specimens and a set of FSTs on an X70 line pipe. A high-speed camera was used to monitor CTOA in both the DWTT and full-scale burst tests on pipes. The experimental results showed that CTOA remains constant during the dynamic crack propagation for X70 pipe at fracture speeds between 80 m/s and 200 m/s. After applied a correction for considering the tilt angle by Xu et al. [32], the averaged surface CTOA values are similar in both DWTT (i.e., 20.1°) and FST (i.e., 20.9°). This indicates that the DWTT measured CTOA is transferable to that for a running crack in the X70 pipeline.

Recently, Sun et al. [33] performed a dynamic fracture simulation of a running crack in a buried gas transmission pipeline using the FEA models to consider the effect of soil constraints and gas decompression on the fracture speed and CTOA. The numerical results showed that the fracture speed decreases with decreasing crack tip pressure, and the CTOA decreases with increasing the soil spring stiffness. Moreover, Bassindale et al. [20] and Zhen et al. [34] improved the Battelle two curve model using the constant CTOA toughness for predicting running fracture arrest for high-grade gas pipelines.

This paper aims to evaluate the constraint independence of CTOA in a different way from those discussed above, where CTOA will be determined from quasi-static fracture toughness tests on SENB specimens with shallow and deep cracks in different constraint conditions at the crack tip. Four CTOA estimation models are introduced for determining a constant CTOA over stable crack growth in the SENB testing. Among them, the ln(P)-LLD linear fit model is similar to that used by ASTM E3039 for calculating CTOA from DWTT specimens. A series of fracture test data for SENB specimens with different crack sizes in high strength ductile steels of X80 and HY80 are considered in the CTOA evaluation. The results show that the proposed CTOA models can determine a crack size or constraint-independent, constant critical CTOA value over stable crack growth in the SENB specimens. This infers that the CTOA measured by ASTM E3039 is constraint-independent and transferable to use for an actual crack propagating in a gas transmission pipeline.

### 2. CTOA Standard Test Methods

# 2.1. CTOA Definition

In fracture mechanics methods, CTOA is defined as the angle between two crack faces of a crack starting from the crack tip. Due to large blunting of a sharp crack for a ductile steel, the original straight

crack faces become curved during plastic deformation. For convenience, the CTOA is simply denoted by an angle,  $\psi$ , and the corresponding total CTOD is denoted by the symbol  $\delta$  at a given distance d from the crack tip, as shown in Fig. 1, the CTOA is mathematically expressed as:

$$\psi = 2\arctan\left(\frac{\delta}{2d}\right) \tag{1}$$

where the distance parameter d is typically given as a small value in the order of 1 mm. If the CTOA value is less than 20°, Equation (1) can be approximated as  $\psi = \delta/d$  with an error less than 1%.

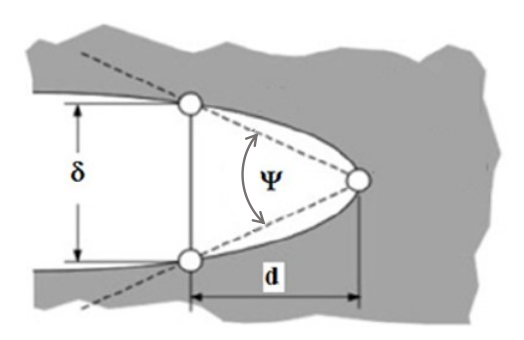


**Figure 1.** Definition of CTOA at a blunt crack tip.

#### 2.2. CTOA Standard Test Method - ASTM E2472

In 2006, ASTM published the first CTOA standard test method with a designation of E2472 [11] for testing CTOA in metallic materials for thin-walled specimens under the low-constraint conditions. This CTOA standard is a direct surface measurement method and determines a constant critical CTOA over stable crack growth using a CT or MT specimen with anti-buckling guides. ASTM E2472 [11] determines an averaged CTOA from Eq. (1) using a four-point method within the specified crack extensions.

To provide a longer uncracked ligament for a larger stable crack growth, different thin-walled bending specimens, such as modified double cantilever beam [MDCB] [13] and DWTT [35], were employed to measure CTOA for pipeline steels in guidance of ASTM E2472 [11]. The test results showed that these two specimens determined comparable CTOA values. Xu et al. [35] pointed out that DWTT specimens are suitable for a mill test, and MDCB specimens are more suitable for laboratory testing for supporting the DWTT CTOA test.

#### 2.3. CTOA Standard Test Method - ASTM E3039

In 2016, ASTM developed a second CTOA standard test method with a designation of E3039 [25] for testing fracture propagation toughness in terms of constant CTOA using the DWTT specimen. This standard method is applicable to ferritic steels exhibiting ductile fracture with 85% and more shear area. This CTOA test standard may meet the technical needs for improving the CVN-based fracture control technology for managing modern gas transmission pipelines. The critical CTOA is defined at the midplane (B/2) of the DWTT specimen and calculated by:

$$CTOA_{\frac{B}{2}} = \frac{8r_p}{\xi} \frac{180}{\pi} (degree)$$
 (2)

where  $r_P$  is a rotation factor with an approximate constant of 0.55, and  $\xi$  is the absolute value of the slope of  $\ln(P/P_m)$  vs  $(\Delta-\Delta_m)/S$  curve with specified data corresponding to  $\ln(P/P_m)$  values between -0.5 to -1.2. Here,  $P_m$  is the maximum applied force, and  $\Delta_m$  is the load-line displacement (LLD) at  $P_m$ . The steady-state region of crack growth assumes to occur between  $P/P_m = 0.60$  and  $P/P_m = 0.30$ .

Numerical analysis [36] showed that the CTOA values obtained by the FEA calculation using Eq. (2) are in good agreement with the values of CTOA $_{B/2}$  calculated at the midplane of the DWTT specimen from the experiment. Results showed that the midplane CTOA $_{B/2}$  is smaller than the surface CTOAc determined by ASTM E2472 [11].

#### 2.4. Constant CTOA Simulation

In addition to the CTOA test methods and experimental studies, extensive numerical simulations were also performed to study the constant CTOA for various ductile steels [22, 36-37]. Numerical simulations can determine more accurate CTOA values over stable crack growth for different fracture specimens, including CT, SENB, MT, MDCB and DWTT. Once the constant critical CTOA $_c$  ( $\psi_c$ ) toughness and a crack driving force in terms of CTOA are obtained for a given crack, the crack stability can be assessed using the CTOA fracture criterion: CTOA  $\leq \psi_c$ . This work aims to determine a single, constraint independent, constant CTOA toughness value for high strength ductile steels rather than a CTOA crack driving force.

# 3. CTOA Estimation Models for SENB Specimens

Both SENB and DWTT are three-point bending specimens, but an SENB has smaller specimen sizes than a DWTT. For the same shallow crack ratio, these two bending specimens may have the similar mechanics behavior at the crack tip, such as constraint conditions and stable constant CTOA at the midplane. This section introduces four indirect estimation models to evaluate the midplane CTOA from fracture toughness testing on SENB specimens in the plane strain conditions.

#### 3.1. CTOA Estimation from Load-Displacement Data

Recently, Zhu et al. [38] developed four CTOA estimation models for SENB specimens under the plane strain conditions. Among which, the first three models were based on the load-LLD data and the plastic hinge model, as recommended by BS 7448-1 [39], and the fourth model was based on the measured J-R curve. Figure 2 plots the plastic hinge model for an SENB specimen with a growing crack, where a small incremental LLD  $(d\Delta)$  generates a small incremental CTOD  $(d\delta)$  at the crack tip, a small incremental crack extension (da), and a small rotation angle  $(d\theta)$ . The distance from the crack tip to the rotation center is denoted as  $r_p b$ , with b = W - a the ligament size and  $r_p$  the plastic rotation factor. For standard SENB specimens with a deep crack ratio within  $0.45 \le a/W \le 0.70$ , the plastic rotation factor  $r_p = 0.44$  [39]. For shallow cracked SENB specimens,  $r_p$  may depend on crack size and strain hardening rate of the material [4]. This case will not be discussed in this work.

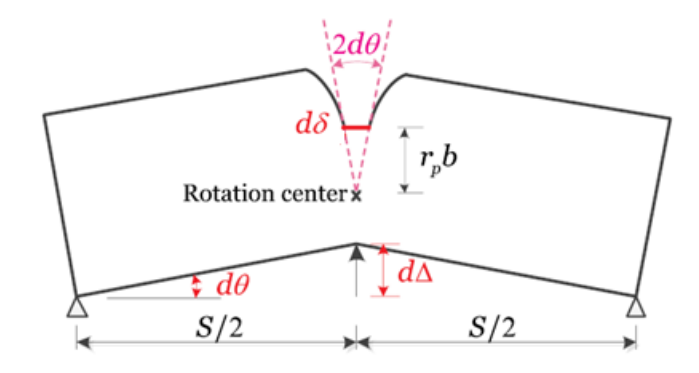


Figure 2. Plastic hinge model for an SENB specimen.

The rigid plastic model requires the material being perfectly plastic. For an SENB specimen in a perfectly plastic material, an applied load can be approximated as a limit load at the post yielding:

$$P = \frac{\lambda \sigma_f B(W - a)^2}{S} \tag{3}$$

where  $\lambda$  is a constant,  $\sigma_f$  is the flow stress defined as an averaged yield strength and ultimate tensile strength, B is the specimen thickness, W is the specimen width, a is the crack length and S is the specimen span. For the limit load analysis of SENB specimens under the plane strain conditions, the constant parameter  $\lambda = 1.455$  [38]. For a strain hardening material, however,  $\lambda$  may depend on the strain hardening exponent of the material. In a single specimen test, applied load and crack length are recorded during the testing, and thus the constant parameter  $\lambda$  can be estimated from the test data and Eq. (3).

From Fig. 2, two simple geometrical relations are obtained as:

$$d\theta = \frac{d\Delta}{S/2} \tag{4}$$

$$d\delta = 2r_p b d\theta \tag{5}$$

From the CTOA definition shown in Fig. 1, when the distance d is replaced by da and  $\delta$  is replaced by  $d\delta$ , the resulted CTOA in Eq. (1) can be rewritten as:

$$\tan\left(\frac{\psi}{2}\right) = \frac{d\delta}{2da} \tag{6}$$

$$\tan\left(\frac{\psi}{2}\right) = \frac{d\delta}{2da} \tag{6}$$
 From Eqs. (4) to (6), one obtains the following relationship between CTOA, LLD and crack extension: 
$$\tan\left(\frac{\psi}{2}\right) = \frac{2r_p b}{s} \frac{d\Delta}{da} \tag{7}$$

From Eq. (3), one obtains the following differential load, dP:

$$dP = -\frac{2\lambda\sigma_f Bb}{\varsigma} da \tag{8}$$

From Eqs. (7) and (8), after eliminating crack extension da, one obtains CTOA as a function of load and the slope of the load-LLD curve:

$$\tan\left(\frac{\psi}{2}\right) = -\frac{4r_p P}{S} \frac{d\Delta}{dP} \tag{9}$$

When  $\psi \le 20^\circ$ ,  $\tan(\psi/2) \approx \psi/2$  with an error less than 1%.

Assuming the crack stably grows from Point 1 ( $P_1$ ,  $\Delta_1$ ,  $a_1$ ) to Point 2 ( $P_2$ ,  $\Delta_2$ ,  $a_2$ ) on the P-LLD curve after the peak load, and CTOA maintains a constant critical value ( $\psi_c$ ) during stable crack growth. In this situation, Equation (9) will further derive three load-LLD based CTOA models, as discussed below.

# Model 1: P-LLD linear fit model

For a linear portion of P-LLD data between Point 1 and Point 2, a linear curve fit can be expressed as:

$$P = k\Delta + c \tag{10}$$

where k and c are the linear curve fit constants. From Eqs. (9 and (10), one obtains the critical CTOA as:

$$\tan\left(\frac{\psi_c}{2}\right) = -\frac{4r_p}{s} \left(\Delta + \frac{c}{k}\right) \tag{11}$$

# Model 2: Ln(P)-LLD linear fit model

Assume the peak load point ( $P_{max}$ ,  $\Delta_{max}$ ) located on the P-LLD curve. Equation (9) can be expressed in the following format:

$$\tan\left(\frac{\psi_c}{2}\right) = -4r_p \frac{d(\Delta - \Delta_{max})/S}{d\left(Ln\left(\frac{P}{Pmax}\right)\right)}$$
(12)

Using the linear regression to curve fit the linear portion of the logarithmic load-LLD data from Point 1 to Point 2, Eq. (12) can be used to calculate  $\psi_c$ . If a small CTOA (i.e.,  $\psi_c \le 20^\circ$ ),  $\tan(\psi_c/2) \approx \psi_c/2$ , and Eq. (12) reduce to Eq. (2), as recommended by ASTM E3039 for DWTT specimens.

# Model 3: Ln(P)-LLD exponential fit model

Reformate Eq. (9) in the following functional form of ln(P) - LLD:

$$\tan\left(\frac{\psi}{2}\right) = -\frac{4r_p}{s} \frac{d\Delta}{d(\ln(P))} \tag{13}$$

where an exponential function between ln(P) and LLD is assumed as the best-fitted curve from Point 1 to Point 2 on the measured data curve. Originally, Zhu et al. [38] assumed a 4<sup>th</sup>-order polynomial function to curve fit the Ln(p)-LLD data over stable crack growth, but this work found that an exponential fit function,  $Ln(p) = C_1 Exp(C_2 * LLD)$  with C<sub>1</sub> and C<sub>2</sub> being curve fit constants, determines a better stable constant CTOA, as demonstrated in Section 5. Note that all three load-LLD models in Eqs. (11) – (13) contain only the rotation factor  $r_P$ , but not the  $\lambda$  parameter.

# 3.2. J-Differential Estimation Method - Model 4

In a fracture toughness test for ductile steels, the J-R curve is evaluated using the incremental J-integral equation as recommended in ASTM E1820 [6], where the applied load (i.e., force), LLD, and crack length data are measured for a growing crack in a single specimen test. For a quasi-statical crack, the differential of the J-integral is expressed as [40]:

$$dJ = \frac{\eta}{Bb} P d\Delta - \gamma \frac{J}{b} da \tag{14}$$

where  $\eta$  and  $\gamma$  are two LLD-based geometrical factors as a function of a/W.

From Eq. (14),  $d\Delta/da$  can be determined. Then from Eq. (7), the following J-differential equation is obtained for estimating CTOA from a J-R curve:

$$\tan\left(\frac{\psi}{2}\right) = \frac{2r_p}{\eta\lambda\sigma_f}\left(\frac{dJ}{da} + \frac{\gamma}{b}J\right) \tag{15}$$

The above equation is Model 4 for the CTOA estimation that was proposed by Zhu et al. [38]. Originally, a J-R curve was assumed to curve fit using a 3<sup>rd</sup> or 4<sup>th</sup> order polynomial function over stable crack growth. This work found that a power law curve fit determines a better constant CTOA, as demonstrated in Section 5.

For standard SENB specimens, the two geometrical factors are often taken as  $\eta$  = 2 and  $\gamma$  = 1. Based on the SENB fracture test data and the J-R curves obtained by Lam et al. [41] for A285 carbon steel, Zhu et al. [38] determined a set of slightly constraint dependent CTOA values from the above-noted four CTOA estimation models with a predetermined  $\lambda$  value. After the fully plastic deformation effect on the  $\lambda$  parameter is correctly considered, a more accurate  $\lambda$  value was obtained for the A285 SENB specimens, and a constrain independent, constant critical CTOA was determined based on the four CTOA estimation models for the A285 carbon steel during stable crack growth [42]. This work aims to apply the four CTOA estimation models to determine the critical CTOA values during stable crack growth for X80 and HY80 high strength ductile steels.

Recently, Lu and Wang [43-44] proposed another CTOA estimation model based on the K-R curve for a growing crack in a large thin-walled CT or MT specimen. This critical CTOA estimation requires the elastically predominated deformation conditions to maintain around the growing crack tip and is applicable only to thin-walled aircraft fuselage structures rather than thicker gas pipelines.

# 3.3 Comparisons of four CTOA models

As discussed above, four CTOA models were proposed by Zhu et al. [38] for evaluating the critical CTOA during the stable crack growth for SENB specimens. Among these CTOA models, the first three were based on the load-displacement data that are specifically applicable to SENB specimens (possible for DWTT specimens), including Model 1 or the P-LLD linear fit model, Model 2 or the Ln(P)-LLD linear fit model, and Model 3 or the Ln(P)-LLD exponential fit model. Results in Section 5 show that these three CTOA models predict comparable results on average, where Model 1 predicts a linearly distributed CTOA values over the region of interest, Model 2 is equivalent to the CTOA model recommended by ASTM E3039 for DWTT specimens and predicts a constant CTOA value over the region of interest, and Model 3 predicts nonlinearly distributed CTOA values over the region of interest. Model 4, namely the J-differential CTOA

estimation model, is completely different from the first three CTOA models. This model provides a physical relationship between the J-integral and the CTOA and predicts the CTOA value from the corresponding J-R curve. Model 4 may be applicable to any fracture specimen provided the four geometry parameters of  $\eta$ ,  $\gamma$ ,  $\lambda$ , and  $r_P$  are available to that fracture specimen.

# 4. Fracture Resistance Testing Using SENB Specimens

# 4.1. Fracture Resistance Testing for X80 Pipeline Steel

Six SENB specimens were tested by Shen et al. [45] at room temperature (i.e.,  $20 \, ^{\circ}$ C) for developing J-R curves for X80 pipeline steel in guidance of ASTM E1820 [6], where initial crack lengths varied to achieve different constraint levels at the crack tip in the plane strain conditions. These SENB specimens were machined from a 48-inch X80 pipe. Chemical compositions of this material were given by Shen et al. [45]. The uniaxial tensile test obtained the 0.2% offset yield stress of 570 MPa (82.7 ksi) and the ultimate tensile stress (UTS) of 675 MPa (97.9 ksi), leading to the flow stress ( $\sigma_f$ ) = 622.5 MPa (90.3 ksi) and Y/T = 0.844. This indicates that X80 is a high strength carbon steel with a low strain hardening rate.

All SENB specimens have a width W = 23 mm, thickness B = W/2 = 11.5 mm, net thickness  $B_N = 9.2$  mm due to a 10% side groove on each side, and the beam span S = 4W = 92 mm. These SENB specimens were pre-cracked by fatigue under applied loading conditions of three-point bending. After pre-cracking, the initial crack ratios, a<sub>0</sub>/W, of the six SENB specimens were measured as 0.24, 0.25, 0.42, 0.43, 0.63, and 0.64. These SENB specimens are thus categorized as two shallow, two intermediate, and two deep-cracked fracture specimens.

Figure 3 shows the test data of load - LLD recorded for the six X80 SENB specimens with  $a_0/W = 0.24$  to 0.64 [45].

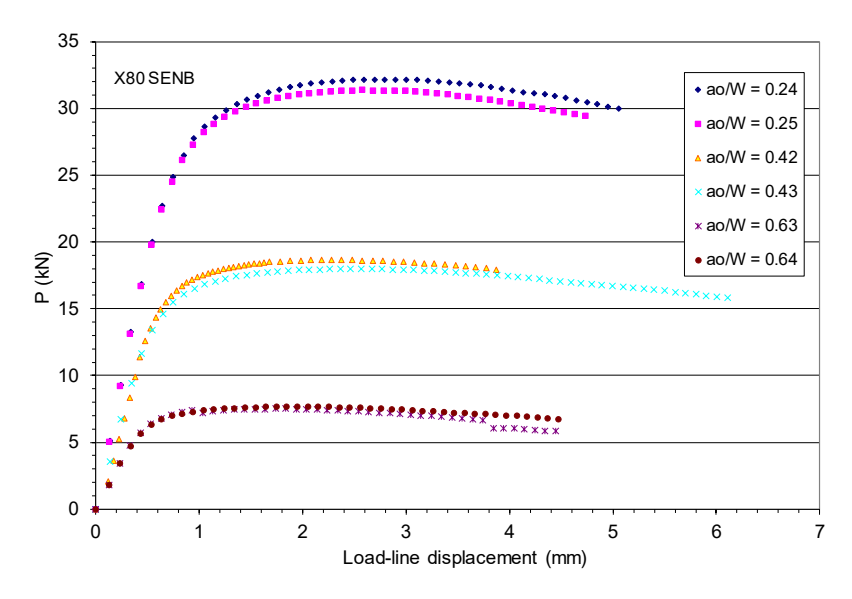


Figure 3. Experimental P-LLD data for six X80 SENB specimens.

As shown in Fig. 3, all six SENB specimens initially experience linearly elastic response, where the load linearly increases with the LLD. Then, the plastic strain hardening occurs and the applied load nonlinearly increases with the plastic deformation up to the maximum load and then drops until the testing is terminated or the specimen fails. The maximum load of these SENB specimens decreases dramatically as

the initial crack length increases. For the shallow crack of, For example, the maximum load  $P_{max} = 32.2 \text{ kN}$ , 18.6 kN, and 7.5 kN, respectively for  $a_0/W = 0.24$ , 0.42, the maximum load and 0.63.

Figure 4 shows the experimentally measured J–R curves [45] that were developed by following the ASTM E1820 fracture test procedures based on the load, LLD and crack length data obtained during the fracture test, where the crack length was measured using the elastic unloading compliance method. Figure 4 clearly shows a crack size-dependence of the J-R curves or the constraint effect on the J-R curves for the X80 pipeline steel. The fracture toughness test results show that the initiation fracture toughness  $J_{Ic} \approx 400$  kJ/m² for the X80 steel.

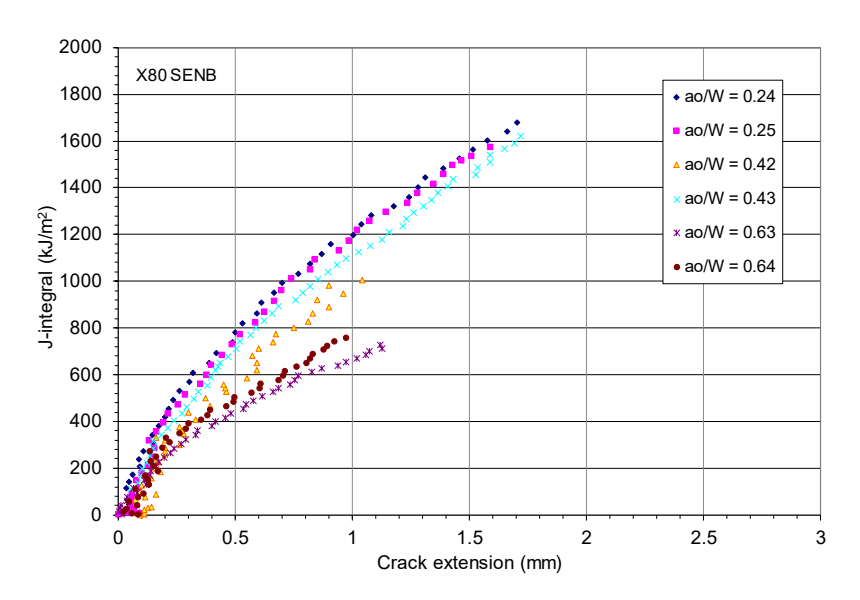


Figure 4. Experimentally measured J–R curves for six X80 SENB specimens.

Initially, this work intended to use the measured P-LLD data and experimental J-R curves for the X80 SENB specimens to evaluate the above-noted CTOA models. However, Figure 4 shows that the crack extensions in all X80 SENB fracture tests are too short, and the stable crack growth may not start for these cracks, particularly for the deep cracks. As a result, these X80 SENB test data are not adequate to use for a constant critical CTOA evaluation.

Recently, Zhen et al. [46] performed a series of FEA simulations of crack propagation for SENB, CT and MDCB specimens with a wide range of initial crack lengths in X80 pipeline steel. The yield strength of this X80 steel is 582 MPa (84.4 ksi) and the UTS is 696 MPa (100.9 ksi). These material properties are similar to those for the X80 pipeline steel used by Shen et al. [45], and thus the fracture toughness properties should be comparable for these two X80 pipeline steels. The numerical simulations aimed to determine the constraint effect on the critical CTOA during stable crack tearing due to different specimen sizes, crack sizes and specimen configurations. In order to simulate crack propagation, these authors adopted ABAQUS/Explicit solver [47] and the micromechanics damage GTN model developed by Gurson [48] and Tevergaard and Needleman [40] in all elastic-plastic FEA simulations in both 2D plane strain conditions and 3D conditions.

Figure 5 shows the FEA numerical results of CTOD values during crack growth obtained by Zhen et al. [46] for the X80 SENB specimens in the 2D plane strain conditions, where three specimen widths of W = 16 mm, 32 mm, and 64 mm and seven initial crack depth ratios of  $a_0/W = 0.1$ , 0.125, 0.15, 0.2, 0.3, 0.5, and 0.7 were employed in their FEA simulations of crack propagation. Figure 5 shows that 1) all CTOA-resistance curves have an initially high value and then a sudden drop in the early crack extension, 2) all

cracks grow into the steady-state extension at  $\Delta a/(W-a_0) \approx 0.2$ , 3) the constant steady-state value of CTOA is ~  $10^{\circ}$  degrees on average within the crack growth region of interest, 4) the thinnest specimen (W=16 mm) with  $a_0/W=0.5$  has a slightly larger CTOA value, and 5) all deep cracks seem to have a hook-up CTOA trend at the end of stable crack growth. From these observations, Zhen et al. [46] concluded that "the arrest toughness CTOAc for X80 pipeline steel is not sensitive to the change of in-plane constraint levels at the crack tip for SENB and CT specimens".

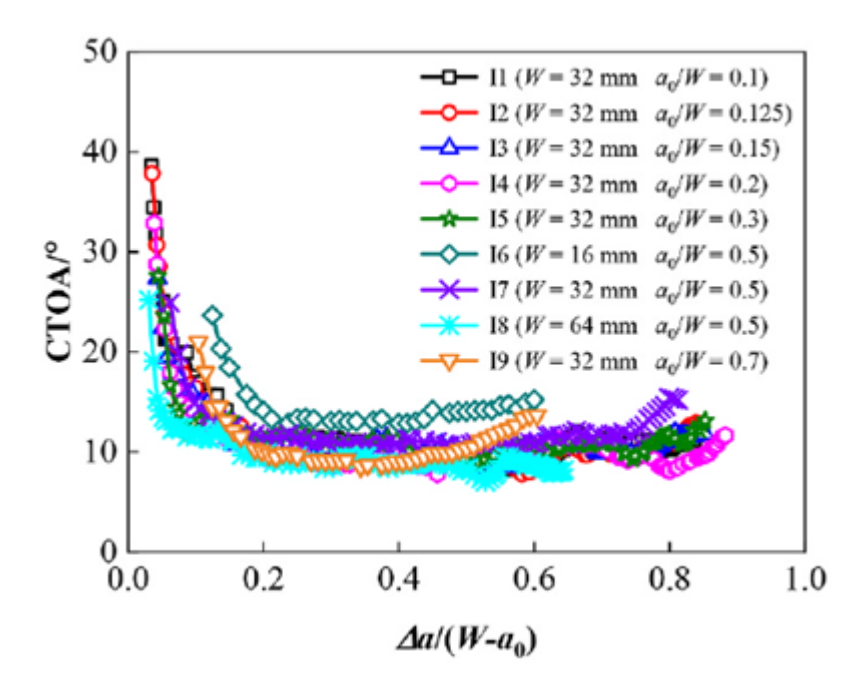


**Figure 5.** Numerical results of CTOA during crack growth determined from X80 SENB specimens with different crack sizes.

As for the starting point of the stable crack growth,  $\Delta a/(W-a_0) \approx 0.2$ , as shown in Fig. 5, it represents the start of stable ductile crack growth at  $\Delta a \approx 1.6$  mm for W=16 mm and  $a_0/W=0.5$ ,  $\Delta a \approx 3.2$  mm for W=32 mm and  $a_0/W=0.5$ , and  $\Delta a \geq 4.48$  mm for all other crack sizes of the X80 SENB specimens. Comparison of these starting points of stable ductile crack growth with the maximum crack extensions measured by Shen et al. [45], as shown in Fig. 4, it confirms that their fracture test data on the X80 SENB specimens, including the measured load-LLD data shown in Fig. 3 and the experimental J-R curves shown in Fig.4, are not sufficient to quantify the corresponding constant critical CTOA value.

### 4.2. Fracture Resistance Testing for HY80

As an alternate to the X80 pipeline steel used by Shen et al. [45], an HY80 structural steel [50] is considered here because these two steels are high strength ductile steels, having the same minimum nominal yield stress of 80 ksi (552 MPa). While X80 is a high strength pipeline carbon steel, HY80 is a high yield (HY) strength submarine steel with low carbon and low alloy and has been used for shipbuilding for more than 55 years [51].

A series of fracture toughness test results was reported by Joyce and Link [50] in 1997 for HY80 steel. All fracture tests were conducted on HY80 SENB specimens at room temperature (21 °C) in guidance of ASTM E1820 [6], where initial crack lengths were varied from shallow to deep for developing different constraint levels at the crack tip. The SENB specimens were machined from 27-mm thick plate in an HY80

steel. Chemical compositions of this material were provided in Ref. [50]. The uniaxial tensile test determined the 0.2% offset yield stress of 630 MPa (91.4 ksi) and the UTS of 735 MPa (106.6 ksi), leading to the flow stress ( $\sigma_f$ ) = 682.5 MPa (99.0 ksi) and Y/T = 0.857. This high Y/T ratio indicates that HY80 is a low strain hardening steel, as X80.

All HY80 SENB specimens have a 1T standard specimen width W = 50.8 mm (2 in.), specimen thickness B = W/2 = 25.4 mm (1 in.), net thickness  $B_N = 20.32$  mm (0.8 in.) due to a total 20% of side grooves, and the beam span S = 4W = 203 mm (8 in.). These SENB specimens were pre-cracked by fatigue in three-point bending. After pre-cracking, the initial crack ratios,  $a_0/W$ , of the SENB specimens were measured to vary in the range of 0.135 to 0.83. In general, deep cracks in the SENB specimens generate high constraint levels at the crack tip, and shallow cracks in the SENB specimens generate low constraint levels at the crack tip.

Figure 6 shows the test data of load – LLD measured during the fracture toughness testing on thirteen HY80 SENB specimens with  $a_0/W = 0.135$  to 0.83 [50].

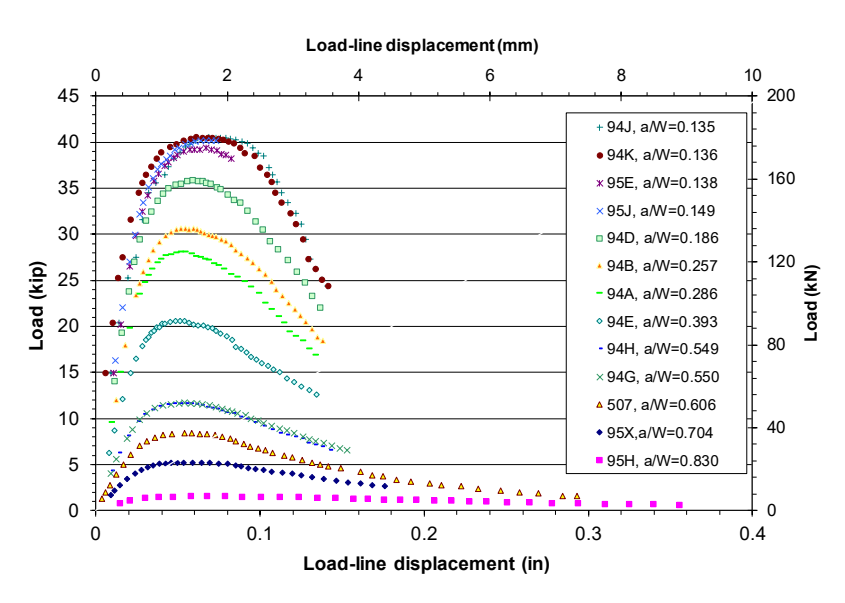


Figure 6. Experimental P-LLD data for a series of HY80 SENB specimens.

As shown in Fig. 6, the applied load linearly increases with LLD initially for all HY80 SENB specimens. Then, plastic strain hardening occurs and the applied load increases nonlinearly with LLD up to the maximum load and then drops until the specimen fails. The maximum load of these SENB specimens decreases dramatically as the initial crack length increases. For example, the maximum load  $P_{max} = 180.2$  kN, 91.8 kN, and 37.3 kN, respectively for  $a_0/W = 0.136$ , 0.393, and 0.606.

In the original fracture toughness testing using HY80 SENB specimens, the elastic unloading compliance method as recommended by ASTM E1820 [6] was adopted for monitoring crack length and for determining crack growth. Experimentally measured J-R curves were reported by Joyce and Link [50] for all HY80 SENB specimens. It should be noted that their experimental J-R curves for shallow-cracked SENB specimens with an JW  $\leq$  0.282 may be incorrect because a negative  $\gamma$  factor was used for the shallow cracks. In the J-R curve evaluation described by ASTM E1820 [6], the  $\eta$  factor equation is used for calculating incremental deformation J-integral at the current load step, and the  $\gamma$  factor is used for crack growth correction on the increment of the J-integral. This implies that the  $\gamma$  factor must be positive because a negative  $\gamma$  factor increases the deformation J-integral, which has no physical meaning, see Zhu and Joyce [52] for more discussions. Because of this reason, the original J-R curves developed by Joyce and Link [50] are not reported here.

Ten years later in 2007, Zhu and Joyce [52] revisited the fracture toughness testing on HY80 SENB specimens and redetermined the crack lengths and J-R curves using the normalization method as recommended in Annex 15 of ASTM E1820 [6]. Note that more accurate expression of the  $\eta$  factor was developed, and a non-negative expression of the  $\gamma$  factor was obtained by Zhu and Joyce [52]. These new expressions of the  $\eta$  and  $\gamma$  factors were used in the J-R curve reevaluation. Figure 7 shows the experimental J-R curves that were developed by Zhu and Joyce [52] by following the ASTM E1820 procedures and based on the applied load, LLD and crack length obtained from the fracture tests, where the crack length was estimated using the normalization method.

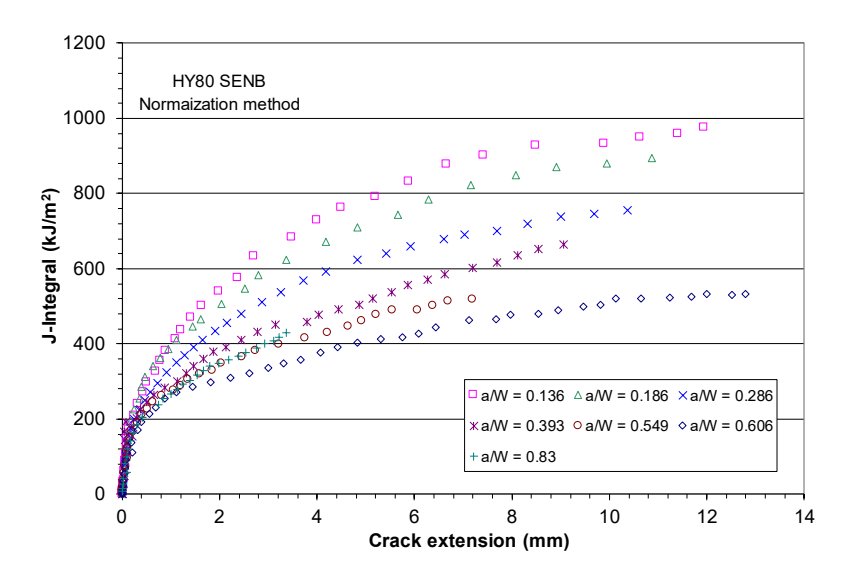


Figure 7. Experimental J–R curves for a set of HY80 SENB specimens.

Figure 7 clearly shows a strong specimen size-dependence of the J-R curves for the HY80 steel, where the in-plane constraint level at the crack tip has a significant effect on the fracture resistance curves. The fracture test results show that the initiation fracture toughness  $J_{Ic} \approx 200 \text{ kJ/m}^2$  from the standard SENB specimens for the HY80 steel. Compared to the initial fracture toughness  $J_{Ic} \approx 400 \text{ kJ/m}^2$  for the X80 steel, it is revealed that the HY80 submarine steel has significantly lower fracture toughness than that for the X80 pipeline steel although these two steels have a similar high yield strength of 80 ksi.

Recall that ASTM E1820 [6] requires the standard SENB specimens having initial crack sizes within  $0.45 \le a_0/W \le 0.7$ . Figure 7 shows that all non-standard SENB specimens with  $a_0/W < 0.45$  or  $a_0/W > 0.7$  determined elevated J-R curves compared to the standard conservative J-R curves for HY80 SENB specimens with  $a_0/W = 0.549$  and 0.606.

As shown in Fig. 7, all crack extensions for the HY80 SENB specimens are larger than 7 mm that is much larger than those at the starting point of stable ductile crack growth, as shown in Fig. 5 for X80. Therefore, these HY80 SENB fracture test data would be adequate for a constant CTOA evaluation against a longer stable crack growth for HY80.

#### 5. Constant CTOA Determination for HY80

# 5.1. Determination of $\lambda$ Parameter

In Eq. (15), the J-differential method requires the  $\lambda$  parameter for calculating CTOA over stable crack extension. The  $\lambda$  parameter in Eq. (3) is a predefined constant for a perfectly plastic material but may depend on the strain hardening exponent of the material for a strain hardening material. The  $\lambda$  parameter

can be estimated from the applied load and crack size data measured during fracture testing. From test data, the  $\lambda$  parameter can be calculated for each specimen over the entire deformation, as shown in Fig. 8.

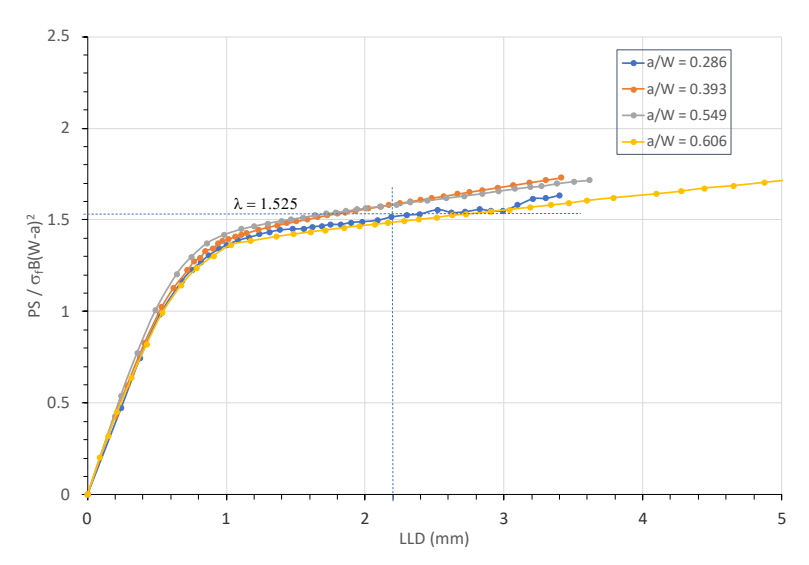


**Figure 8.** Variation of  $\lambda$  parameter with LLD for four HY80 SENB specimens.

It is seen from Fig. 8 that the calculated  $\lambda$  value varies from 1.25 to 1.75 during the plastic deformation and is nearly independent of crack sizes. Figure 6 shows that for all SENB tests, LLD  $\approx$  2.4 mm corresponds a stable crack growth stage, where an approximate linear relation exists between load and LLD. At this LLD,  $\lambda$  = 1.525 is estimated from Fig. 8. This  $\lambda$  parameter value will be used in this work for the critical CTOA evaluation for the HY80 steel.

Figure 9 shows variations of the applied load P and the limit load solution from Eq. (3) with the ligament-squared size  $(1-a/W)^2$  during the entire deformation, including initial elastic deformation and plastic deformation during the crack growth. In Fig. 9, both the applied and limit loads are normalized using  $\sigma_f$  BW<sup>2</sup>/S. This figure includes two limit load solutions, one uses the estimated  $\lambda$  = 1.525 for HY80 steel, and the other uses  $\lambda$  = 1.455 for a perfectly plastic material. For each HY80 SENB specimen, the normalized applied load increases quickly from an initially small load in the elastic deformation condition to the maximum load at the full plastic deformation condition, and then decreases gradually in a linear manner due to stable crack growth. The crack growth direction is marked in Fig. 9. Clearly, the limit load solution with  $\lambda$  = 1.525 is better to match the experimental data and to describe the fully plastic conditions for the HY80 SENB specimens compared to  $\lambda$  = 1.455 for the perfectly plastic material. Thus,  $\lambda$  = 1.525 is selected to use hereafter.

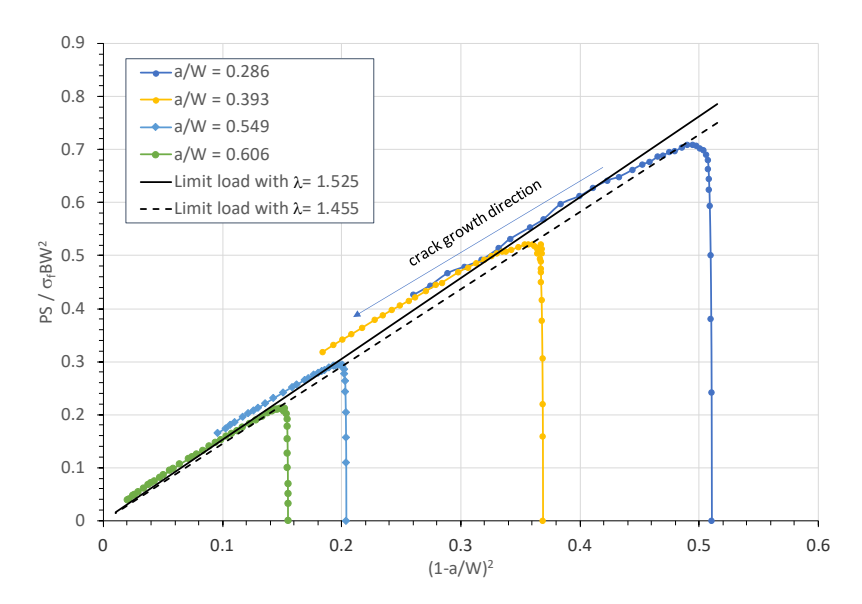


**Figure 9.** Comparison of limit load with applied load in fracture tests for four HY80 SENB specimens.

## 5.2. CTOA for HY80 SENB with $a_0/W = 0.606$

This section determines the critical CTOA value for each HY80 SENB specimen in terms of Model 1 in Eq. (11), Model 2 in Eq. (12), Model 3 in Eq. (13), and Model 4 in Eq. (15). To quantify the constraint effect on the critical CTOD, four HY80 SENB tests are selected and analyzed in this section. This includes the crack sizes of  $a_0/W = 0.606$ , 0.549, 0.393, and 0.286 for the HY80 SENB specimens. These four crack sizes reflect different constraint effects on J-R curves, as shown in Fig. 7, and describe high to low constraint levels at the crack tip for the HY80 SENB specimens.

It is commonly known that experimental test data always contain certain variations due to measurement noises, and thus a smoothed best-fit curve is needed for determining the first-order derivative of the best-fit curve.

- 1) For Model 1, the linear curve fit is used to simply fit the experimental data exhibiting a linear relation on the measured P-LLD curve, and then CTOA is calculated from Eq. (11).
- 2) For Model 2, the peak load point ( $P_{max}$ ,  $\Delta_{max}$ ) is first located, and then  $Ln(P/P_{max})$  and  $(\Delta-\Delta_{max})/S$  are calculated from the peak load point to the final measured point. The linear regression is used to fit the linear portion of  $Ln(P/P_{max})$  vs  $(\Delta-\Delta_{max})/S$  data, and then CTOA is calculated from Eq. (12).
- 3) For Model 3, Ln(P) is first calculated, and an exponential function is curve fitted on the Ln(P)-LLD data. The first-order derivative of the exponential curve is calculated, and then CTOA is determined from Eq. (13).
- 4) For Model 4, a power law function is first curve fitted using the nonlinear regression method from a J-R curve obtained in the fracture test. Then, the first-order derivative of the power law J-R curve is calculated, and finally CTOA is determined from Eq. (15).

Using the above-noted procedures, the CTOA resistance curves (or constant CTOA) against stable crack growth can be determined using the three load-LLD based models and the J-differential model. Figure 10 plots the CTOA resistance curves against crack extension, where the CTOA values are obtained using Models 1, 2, 3, and 4, respectively for the HY80 SENB specimen with the deep crack of  $a_0/W=0.606$ . It is seen that all proposed models determine comparable critical CTOA values over the range of stable crack extension from  $\Delta a = 2.0$  mm to 6.2 mm. It is observed that over the stable crack growth zone: (1) Model 2

determines a constant CTOA,  $\psi_c$  = 3.20°, (2) Model 1 determines a linearly decreasing CTOA with an average value of  $\psi_c$  = 3.18° with the R-square value of 0.9982, (3) Model 3 determines a nearly constant CTOA with an average value of  $\psi_c$  = 3.19° with the R-squared value of 0.9982, and (4) Model 4 can determine a CTOA over a large crack growth, and the CTOA curve becomes nearly flat over the stable crack growth zone with an average value of  $\psi_c$  = 3.10° and the squared value is 0.9827. These high R-squared values indicate the high curve-fit quality of the predefined curve-fit functions.

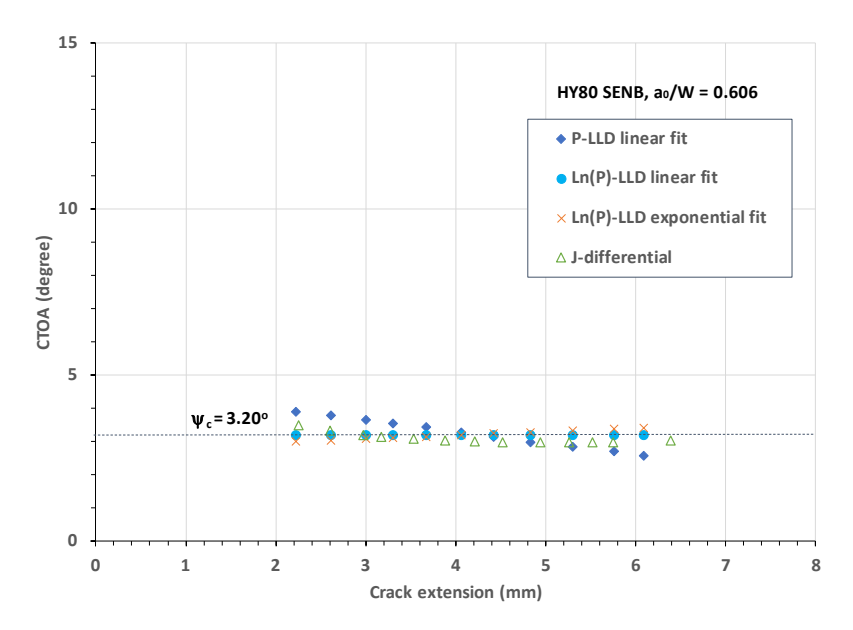


Figure 10. CTOA resistance against crack extension for HY80 SENB specimen with  $a_0/W = 0.606$ .

# 5.3. CTOA for HY80 SENB with $a_0/W = 0.549$

In the same manner as discussed above, four best curve-fitted functions are obtained and then utilized to calculate CTOA . Figure 11 plots the CTOA resistance against crack extension obtained using the four CTOA models for HY80 SENB specimen with the deep crack of  $a_0/W=0.549$ .

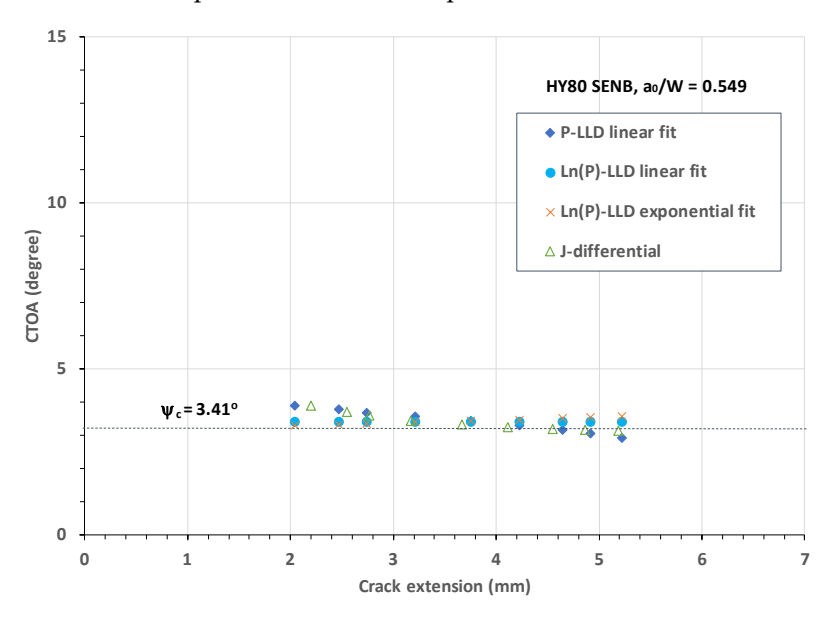


Figure 11. CTOA resistance against crack extension for HY80 SENB specimen with  $a_0/W = 0.549$ .

As evident in Fig. 11, all four CTOA models determine comparable critical CTOA values over the range of stable crack extension from  $\Delta a = 2.0$  mm to 5.0 mm. Figure 11 demonstrates that over the stable crack growth zone, (1) Model 2 determines a constant CTOA,  $\psi_c = 3.41^\circ$ , (2) Model 1 determines a linearly decreasing CTOA with an average value of  $\psi_c = 3.42^\circ$ , (3) Model 3 determines a nearly constant CTOA with an average value of  $\psi_c = 3.43^\circ$ , and (4) Model 4 also determines nearly constant CTOA over the stable crack extension zone with an averaged  $\psi_c = 3.40^\circ$ .

# 5.4. CTOA for HY80 SENB with $a_0/W = 0.393$

In the same manner, four best curve-fitted functions are obtained and employed to determine the CTOA values. Figure 12 plots the CTOA resistance against crack extension obtained from Models 1, 2, 3, and 4, respectively for HY80 SENB specimen with an intermediate crack size of a<sub>0</sub>/W=0.393.

Figure 12 shows that all four CTOA models determine comparable critical CTOA values over the stable crack extension from  $\Delta a = 3.8$  mm to 8.1 mm.

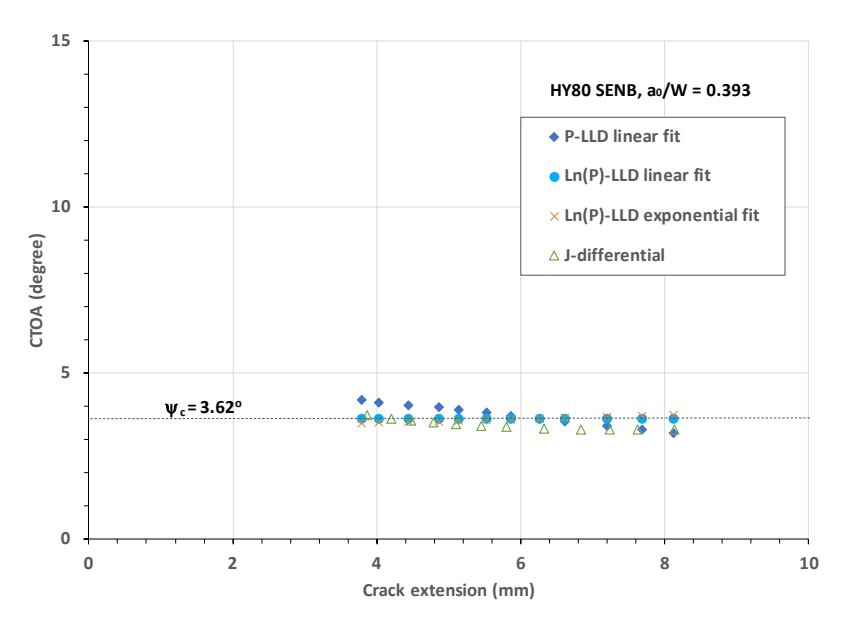


Figure 12. CTOA resistance against crack extension for HY80 SENB specimen with  $a_0/W = 0.393$ .

From Fig. 12, it is observed that over the stable crack extension zone, (1) Model 2 determines a constant CTOA,  $\psi_c$  = 3.62°, (2) Model 1 determines a linearly decreasing CTOA with an average constant value of  $\psi_c$  = 3.63°, (3) Model 3 determines a nearly constant CTOA with an average value of  $\psi_c$  = 3.61°, (4) Model 4 also determines a nearly constant CTOA over the stable crack growth zone with an average constant value of  $\psi_c$  = 3.44°, and (5) Model 4 determines conservative CTOA values over most stable crack extensions. These lower CTOA values may be caused by use of the constant  $\eta$  = 2 for all crack sizes of HY80 SENB specimens because this  $\eta$  value was used in the experimental J-R curve evaluation [52]. If a smaller  $\eta$  value (e.g.,  $\eta$ =1.9 as recommended in the current ASTM E1820) is used, the CTOA value will go up.

#### 5.5. CTOA for HY80 SENB with $a_0/W = 0.286$

In the similar way, Figure 13 shows the CTOA resistance against crack extension obtained from four CTOA models for HY80 SENB specimen with a shallow crack size of ao/W=0.286.

Figure 13 shows that all four CTOA models determine comparable critical CTOA values over the stable crack extension from  $\Delta a = 3.2$  mm to 7.0 mm. From Fig. 13, it is observed that over the stable crack

growth zone, (1) Model 2 determines a constant CTOA,  $\psi_c = 3.19^\circ$ , (2) Model 1 determines a linearly decreasing CTOA with an average constant value of  $\psi_c = 3.21^\circ$ , (3) Model 3 determines an almost constant CTOA with an average value of  $\psi_c = 3.21^\circ$ , and (4) Model 4 determines a slightly decreasing CTOA with an average constant value of  $\psi_c = 3.31^\circ$ . Note that  $\eta = 2$  was used in the original experimental J-R curve evaluation for this shallow crack. In fact, the  $\eta$  factor for this shallow crack is not a constant but may vary with the crack extension.

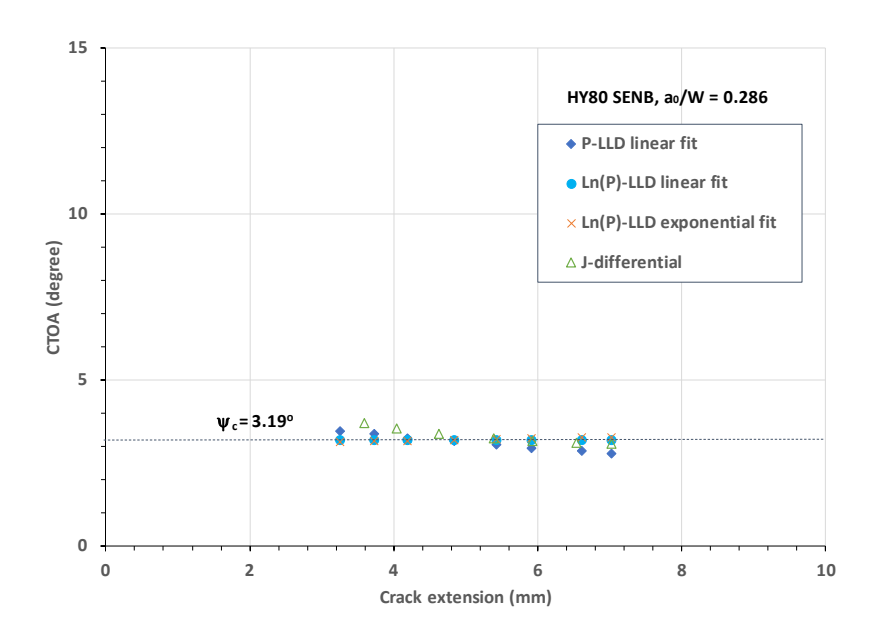


**Figure 13.** CTOA resistance against crack extension for HY80 SENB specimen with  $a_0/W = 0.286$ .

In summary, the above analyses, as shown in Figs. 10 - 13, demonstrate that (1) the Ln(P)-LLD linear fit model (i.e., Model 2) determines a constant CTOA over the stable crack growth for the shallow and deep cracks of HY80 SENB specimens, (2) the P-LLD linear fit model (i.e., Model 1) determines a linearly decreasing CTOA over the stable crack growth for all cracks, (3) the Ln(P)-LLD exponential fit model (i.e., Model 3) determines a nearly constant CTOA over the stable crack growth for all cracks, and (4) the J-differential model (i.e., Model 4) determines a slightly conservative CTOA over stable crack growth. The accurate CTOA results depend on the quality of J-R curve test data and the exponential curve fit over the entire range of crack extension.

# 5.6. Constraint Independence of Critical CTOA

Figure 14 compares the critical CTOA values obtained in this work with crack sizes for the HY80 SENB specimens. As shown in Fig. 14, the crack size or crack-tip constraint level has a small or negligible effect on the critical CTOA value, and the averaged critical CTOA is obtained as 3.35° for the HY80 steel. In contrast, the crack-tip constraint level has a significant effect on the J-R curves for the HY80 steel, as shown in Fig. 7. Therefore, the J-R curves are frequently used to characterize fracture resistance against ductile crack initiation and short stable crack tearing for ductile steels, and the constant CTOA toughness is an adequate fracture parameter utilzed to describe large stable crack growth for high strength ductile steels.

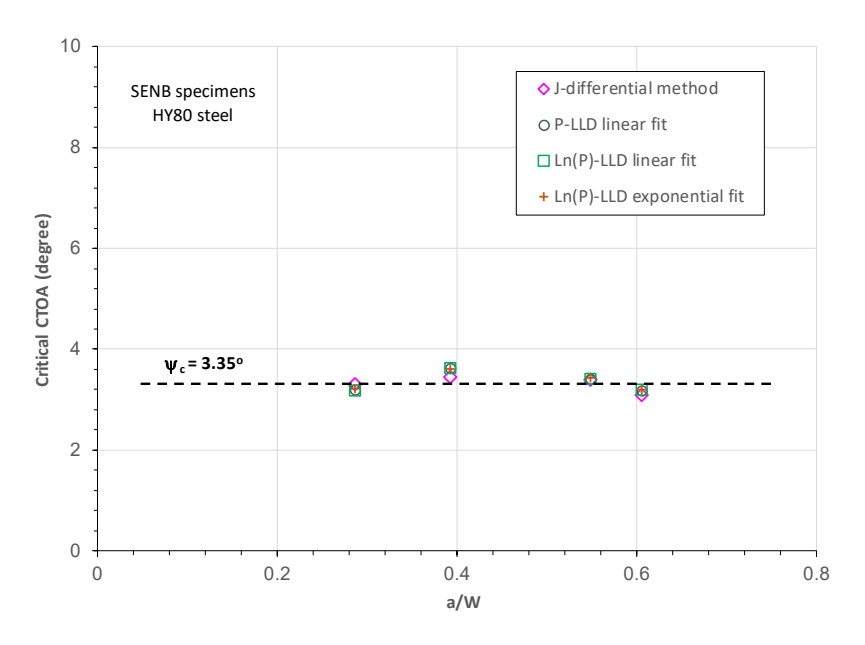


Figure 14. Variations of constant critical CTOA with crack sizes for HY80 SENB specimen

# 6. Conclusions

This paper evaluated the constraint independence of the critical CTOA values that were determined over stable crack growth using the fracture test data for SENB specimens and based on the four CTOA estimation models . A series of experimental test data on the SENB specimens for HY80 structural steel were employed to assess these CTOA models and to determine the constraint independence of the critical CTOA for HY80 steel. From the present study and other available numerical and experimental investigations on the transferability of CTOA measured using the DWTT specimens, the primary results are obtained as:

- The Ln(P)-LLD linear fit model determined a constant critical CTOA over the stable crack growth. The P-LLD linear fit model determined a linearly decreasing CTOA, and the Ln(P)-LLD exponential fit model determined a nearly constant CTOA over stable crack growth. On average, these three load-displacement based models determined comparable CTOA values over stable crack growth.
- 2) Using experimental J-R curve data and a power law curve fit, the J-differential model determined a nearly constant critical CTOA value over stable crack growth. This CTOA value is comparable to those determined from the three-displacement based models. Note that the J-R curves for HY80 steel strongly depends on the constraint levels at the crack tip, whereas its critical CTOA value is essentially independent of the crack-tip constraint levels over stable crack growth. Therefore, the J-R curves are usually used to characterize ductile crack initiation and small stable crack tearing for ductile materials, and the constant critical CTOA is the best fracture parameter for use to describe large stable crack growth for high strength ductile steels.
- 3) The results showed that the Ln(P)-LLD linear fit model is comparable to the CTOA model recommended by ASTM E3039 and determined a constant critical CTOA over the stable crack growth for all cracks of the SENB specimens. The other three CTOA models also determined comparable constant critical CTOA over the stable crack growth.
- 4) Both X80 and HY80 are high strength steels with the similar yield strength of 80 ksi (552 MPa) but have significantly different fracture toughness values. For X80, the fracture toughness  $J_{Ic}$  = 400 kJ/m<sup>2</sup>

- and the critical CTOA =  $10^{\circ}$ . For HY 80, the fracture toughness  $J_{Ic}$  =  $200 \text{ kJ/m}^2$  and the critical CTOA =  $3.35^{\circ}$ .
- 5) The results demonstrated that the constant critical CTOA determined using HY80 SENB specimens is independent of crack size or constraint level at the crack tip. This infers that CTOA measured by ASTM E3039 is constraint-independent, and thus supports the transferability of CTOA measured by ASTM E3039 to an actual crack assessment. Therefore, CTOA is a single, reliable, constant fracture toughness measurement regardless of fracture specimen geometry or constraint level at the crack tip. As a result, the CTOA fracture criterion allows accurate prediction of crack propagation or arrest in complex structures, which improves design analysis and enhances robust material characterization.

Acknowledgments: This work was partially sponsored by U.S. Department of Energy (DOE) Laboratory Directed Research and Development (LDRD) program within Savannah River National Laboratory. This document was prepared in conjunction with work accomplished under Contract No. 89303321CEM000080 with the U.S. DOE Office of Environmental Management (EM).

#### References

- 1. Rice JR. A path independent integral and the approximate analysis of strain concentration by notches and cracks, *Journal of Applied Mechanics*, 1968, 35: 379-386.
- 2. Wells AA. Application of fracture mechanics at and beyond general yielding, *British Welding Journal*, 1963, 10: 563-570.
- 3. Anderson H. A finite element representation of stable crack growth, *Journal of Mechanics and Physics in Solids*, 1973, 21: 337-356.
- 4. Zhu X-K, Joyce JA. Review of fracture toughness (G, K, J, CTOD, CTOA) testing and standardization, *Engineering Fracture Mechanics*, 2012, 85: 1-46.
- 5. ASTM E399-22, Standard Test Method for Linear-Elastic Plane-Strain Fracture Toughness of Metallic Materials. American Society of Testing and Materials International, West Conshohocken, PA, 2022.
- 6. ASTM E1820-22, Standard Test Method for Measurement of Fracture Toughness. American Society of Testing and Materials International, West Conshohocken, PA, 2022.
- 7. Zhu X-K. Review of fracture toughness test methods for ductile materials in low-constraint conditions, *International Journal of Pressure Vessels and Piping*, 2016, 139-140: 173-183.
- 8. Li J, Yu P, Saini N, Li L. Crack-tip opening displacement of girth welds in a lean X70 pipeline steel, *Materials*, 2024, 17, 391.
- 9. Ju J-B, Kim W, Jang J. Variation in DBTT and CTOD within weld heat-affected zone of API X65 pipeline steel, *Materials Science and Engineering A*, 2012: 546: 258-262.
- 10. Newman JC, James MA, Zerbst U. A review of the CTOA/CTOD fracture criterion, *Engineering Fracture Mechanics*, 2003, 70: 371-385.
- 11. ASTM E2472-12e1, Standard Test Method for Determination of Resistance to Stable Crack Extension under Low-Constraint Conditions, American Society of Testing and Materials International, West Conshohocken, PA, 2018.
- 12. Chao YJ, Sutton MA. Accurate measurement of two- and three-dimensional surface deformations for fracture specimens by computer vision, *Experimental Techniques in Fracture* (editor: J.S. Epstein), VCH Publisher, 1993: 59-94.
- 13. Darcis PP, McCowan CN, Windhoff H, McCloskey JD, Siewer TA. Crack tip opening angle optical measurement methods in five pipeline steels, *Engineering Fracture Mechanics*, 2008, 75: 2453-2468.
- 14. Horsley DJ. Background to the use of CTOA for prediction of dynamic ductile fracture arrest in pipelines, *Engineering Fracture Mechanics*, 2003, 70: 547-552.

- 15. Zhu X-K. State-of-the-art review of fracture control technology for modern and vintage gas transmission pipelines, *Engineering Fracture Mechanics*, 2015, 148: 260-280.
- 16. Tyson WR, Newman JC, Xu S. Characterization of stable ductile crack propagation by CTOA: review of theory and applications, *Fatigue and Fracture in Engineering Materials and Structures*, 2018, 41: 2421-2437.
- 17. Ben Amara M, Pluvinage G, Cappelle J, Azari Z. New numerical tools to calibrate the two curves method using the CTOA reiterion, *Engineering Fracture Mechanics*, 2019, 205: 532-546.
- 18. Xu S, Bassindale C, Xue J, Williams BW, Wang X. Recent progress in development of ductile fracture arrest methodology based on CTOA: test standard, transferability and methodology, *Proceedings of the 13th International Pipeline Conference*, September 29-30, 2020, Virtual, Online. IPC2020-9299.
- 19. Zhen Y, Zu Y, Cao Y, Niu R. Effect of accurate prediction of real-time crack tip position on dynamic crack behaviors in gas pipeline, *Journal of Natural Gas Science and Engineering*, 2021, 94: 104136.
- 20. Bassindale C, Wang X, Tyson WR, Xu S, Guan C, Rothwell B. Analysis of full-scale burst test by FE Modelling using constant CTOA fracture criterion, *Journal of Pipeline Science and Engineering*, 2022, 2: 52-59.
- 21. Xu S, Eagleson R, Tyson WR, Park D-Y. Cracking tunnelling and crack tip opening angle in drop-weight tear test specimens, *International Journal of Fracture*, 2011, 172:105-112.
- 22. Xu S, Simha CHM, William BW, Tyson WR. CTOA testing of thick DWTT specimens: experiment and FEA simulation for development of an Annex for ASTM E3039, *Journal of Testing and Evaluation*, 2020, 48(6): JTE20180816.
- 23. Martinelli A, Venzi S. Tearing modulus, J-integral, CTOA and crack profile shape obtained from the load-displacement curve only, *Engineering Fracture* Mechanics, 1996, 153: 263-277.
- 24. Xu S, Bouchard R, Tyson WR. Simplified single-specimen method for evaluating CTOA, *Engineering Fracture Mechanics*, 2007, 74: 2459-2464.
- 25. ASTM E3039-20, Standard Test Method for Determination of Crack Tip Opening Angle of Pipe Steels using DWTT Specimens, American Society of Testing and Materials International, West Conshohocken, PA, 2020.
- 26. Parmar S, Bassindale C, Wang X, Tyson WR, Xu S. Simulation of ductile fracture in pipeline steels under varying constraint conditions using cohesive zone modeling, *International Journal of Pressure Vessels and Piping* 162, 2018: 86-97.
- 27. Zhen Y, Liu Y, Cao Y, Niu R. Study on crack tip opening angle evolutions during dynamic crack propagation of pipelines, *Fatigue & Fracture of Engineering Materials & Structures*, 2023, 46: 1969 1978. FEA constant CTOA, STPG370 low C steel
- 28. Jiao J, Gervasyev A, Barbaro F, Lu C, Rolfe B, Weiss M. Omega and CTOA for dynamic steady-state fracture propagation and their dependency for fracture speed, *Theoretical and Applied Fracture Mechanics*, 2023, 127: 104072.
- 29. Xu S, Bassindale C, Wang X, Tyson WR. Characterization of CTOA for resistance to pipeline ductile fracture propagation, *Journal of Pipeline Science and Engineering*, JPSE100263, January 2025.
- 30. Paermentier B, Gooreman S, et al., A dynamic tensile tear test methodology to characterize dynamic fracture behaviour of modern high-grade pipeline steels, *Engineering Fracture Mechanics*, 2022, 272: 108687.
- 31. Shibanuma K, Hosoe T, Yamaguchi H, Tsukamoto M, Suzuki K, Aihara S. Crack tip opening angle during unstable ductile crack propagation of a high pressure gas pipeline, *Engineering Fracture Mechanics*, 2018, 204: 434-453.
- 32. Xu S, Bassindale C, Williams BW, Wang X, Tyson WR, Shibanuma K. Comments on CTOA transferability in Crack tip opening angle during unstable ductile crack propagation of a high pressure gas pipeline" [204 (2018) 434-453], *Engineering Fracture Mechanics*, 2019, 214: 335-338.
- 33. Sun D, Chen Y, Chao H, Jiang J, Li H, Li Q. A dynamic fracture finite element model of the buried gas transmission pipeline combing soil constraints and gas decomposition, *Engineering Fracture Mechanics*, 2022, 276: 108864.
- 34. Zhen Y, Chang Q, Cao Y, Li F, Wu G. A two-curve model for crack arrest prediction for high-grade pipeline based on crack tip opening angle, *Engineering Fracture Mechanics*, 2022, 217: 108626.

- 35. Xu S, Tyson WR, Eagleson R. Measurement of CTOA of pipeline steels using MDCB and DWTT specimens, *Proceedings of the 8th International Pipeline Conference*, September 27 October 1, 2010, Calgary, Alberta, Canada. IPC2010-31076.
- 36. Gullerud AS, Dodds RH, Hampton RW, Dawicke DS. Three-dimensional modeling of ductile crack growth in thin sheet metals: computational aspects and validation, *Engineering fracture Mechanics*, 1999, 63: 347-374.
- 37. Shuai J, Tu S, Wang J, Ren X, He J, Zhang Z. Determination critical CTOD for energy-load curves with DWTT specimen, *Engineering Fracture Mechanics*, 2017, 186: 47-58.
- 38. Zhu X-K, Lam P-S, Chao YJ. Constraint-dependent CTOA determination for stable ductile crack growth, *Engineering Fracture Mechanics*, 2022, 271: 108651.
- 39. BS 7448-1, Fracture Mechanics Toughness Tests Part 1: Method for Determination of Kic, Critical CTOD, and Critical J Values of Metallic Materials, British Standards Institution, 1991.
- 40. Zhu X-K. Improved Incremental J-Integration Equations for Determining Crack Growth Resistance Curves, *Journal of Pressure Vessel Technology*, 2012, 134: 051404.
- 41. Lam PS, Chao YJ, Zhu XK, Kim Y, Sindelar RL. Determination of constraint-modified J-R curves for carbon steel tanks. *Journal of Pressure Vessel Technology*, 2003, 125: 136-143.
- 42. Zhu X-K. Determination of constraint-independent critical crack tip opening angle during stable crack growth for ductile steels, *Materials Performance Characteristics*, 2024, 13(2): MPC20230087.
- 43. Lu L, Wang S. Relationship between crack growth resistance curves and critical CTOA, *Engineering Fracture Mechanics*, 2017, 173: 146-156.
- 44. Lu L, Wang S. A simple model to explain transferability of crack tip opening angle, *Engineering Fracture Mechanics*, 2018, 193: 197-213.
- 45. Shen G., Tyson WR, Glover A, Horsley D. Constraint effects on linepipe toughness, *Proceedings of the 4th International Conference on Pipeline Technology*, Vol. 2, May 9-13, 2004, Ostend, Belgium, pp. 703-720.
- 46. Zhen Y, Jiao Z, Cao Y, Niu R. Unified correlation of constraints with crack arrest toughness for high-grade pipeline steel, *International Journal of Pressure Vessels and Piping*, 2021, 193: 104454.
- 47. ABAQUS Explicit, Analysis User's Manual, Dassault System Simulia Corporation, Providence, RI, USA, 2020.
- 48. Gurson AL. Continuum theory of ductile rupture by void nucleation and growth: Part I yield criterion and flow rules for porous ductile media, *Journal of Engineering Materials Technology*, 1977, 99(1): 2-15.
- 49. Tvergaard V, Needleman, A. Analysis of the cup-cone fracture in a round tensile bar, Acta Metallurgica, 1984, 32(1): 157-169.
- 50. Joyce JA, Link RE. Application of Two Parameter Elastic-Plastic Fracture Mechanics to Analysis of Structures, *Engineering Fracture Mechanics*, 1997, 57: 431-446.
- 51. Bogdan S, Radoslaw K. Material properties of HY80 Steel after 55 years of operation for FEM applications, *Materials*, 2021, 14: 14154213.
- 52. Zhu X-K, Joyce JA. J-Resistance curve of HY80 steel using SE(B) specimens and normalization Method, *Engineering Fracture Mechanics*, 2007, 74: 2263-2281.